This paper was selected for oral presentation in ICASSP

REGULARIZED TRACKING OF SHEAR-WAVE IN ULTRASOUND ELASTOGRAPHY

Mahmoud Derakhshan Horeh[†], *Amir Asif* [†], *and Hassan Rivaz*[†‡]

[†]Electrical and Computer Engineering, Concordia University, Montreal, QC, Canada H3G 1M8
[‡] PERFORM CENTRE, Concordia University, Montreal, QC, Canada H4B 1R6

ABSTRACT

Ultrasound elastography involves imaging tissue while it undergoes deformation and inferring its mechanical properties from the deformation pattern. The initial deformation in the tissue is typically induced through an external mechanical force, for example, by exerting a slight pressure using an ultrasound probe or by applying an acoustic radiation force (ARF) against the tissue. The ARF excites the tissue locally, which leads to the propagation of a shear-wave. The goal of the shear-wave elastography is to estimate the speed of the shear-wave that is explicitly related to the elasticity of tissue. We formulate tissue displacement estimation as an optimization problem and propose a computationally efficient approach to estimate the displacement field. A novel algorithm based on the minimization of a regularized cost function using higher-order analytical minimization (HAM) coupled with the second-order Taylor series approximation is proposed. Our algorithm first computes an integer displacement field based on dynamic programming (DP) that provides the global optima, which is then refined iteratively to obtain the subpixel displacement estimate. We test the proposed algorithm on real experimental data obtained from a tissue-mimicking phantom and illustrate the superiority of our approach over some commonly used elastography techniques using signal to noise ratio (SNR) comparisons.

Index Terms— Shear-Wave, Analytical Minimization, Regularization, Elastography, Ultrasound, Dynamic Programming.

1. INTRODUCTION

Imaging the tissue elasticity is highly desired in numerous medical applications such as detecting cancerous tumours and guiding biopsies. During the past two decades, several ultrasound (US) imaging techniques have been proposed to estimate the mechanical properties of the tissue [1–3]. These techniques are generally referred to as ultrasound elastography and are broadly categorized into two different groups of quasi-static and dynamic elastography. In quasi-static elastography [4, 5], a slow, relatively static compression is applied to the tissue and the US radio frequency (RF) signals acquired before and after the compression are correlated to estimate tissue displacements. In dynamic elastography [6–9], tissue deformation happens at a much faster rate and the propagation of mechanical waves (compressional or shear in nature) are used to derive the displacements in the tissue. Although both static and dynamic approaches use ultrasound to track the displacements, the difference lies in the applied stress, whether it is quasi-static or due to the propagation of the shear wave. Depending on the type of excitation, dynamic elastography itself can be further categorized into several different subgroups, including shear-wave imaging (SWI), which generates a deep "push" in the tissue by applying a non-invasive acoustic radiation force (ARF) [8–10]. The resulting disturbance propagates sideways through the tissue in the form of a shear wave that can be monitored using the US RF data collected immediately before and after the ARF excitation. In this paper, we focus on dynamic shear-wave elastography through the results are generalizable to other variations of elastography.

Mathematically speaking, the radiation force [10] generated by a propagating acoustic wave in soft tissue is given by

$$F = \frac{2\alpha I}{c} \tag{1}$$

where I denotes the temporal average intensity at a given point in space, α is the absorption coefficient of the medium, and c the speed of sound. The radiation force for a given region of excitation (ROE) is uniform if all three parameters $\{I, \alpha, c\}$ are relatively constant across the ROE. Alternatively, the variations in these parameters represent the inhomogeneity in the medium and can be used to derive the mechanical properties of the tissue.

In SWI, a localized and focused radiation force F is applied to the region of interest to induce a shear wave that travels orthogonal to the probing radiation. When the excitation is focused at a specific tissue site, transient shear waves are propagated away from the ROE [6]. During the propagation phase, the displacement field and the attenuation of the propagating wave, collectively, contain useful information on the local mechanical properties of the tissue. The displacement field in the tissue is often tracked by a transducer [11] housed in an ultrasound machine that produces images of the region at a high frame rate. By comparing successive frames, the tissue displacement (or, alternatively the propagation velocity of the shear wave) can be determined both spatially and temporally using a correlation-based approach [12]. Normalized cross-correlation (NCC) [13], a common approach used for estimating tissue displacement, has shown poor estimation results when applied to radio frequency (RF) data. It also has a significant computational complexity.

An alternative to normalized cross correlation for shear motion estimation is the regularized cost function [14, 15]. These regularization-based approaches calculate subsample displacement and are computationally efficient. In terms of time, they are affordable and appropriate for real-time clinical applications. The paper seeks to further improve the subpixel accuracy of the displacement field estimate over [14, 15] by incorporating a higher order Taylor series expansion into the cost function. As we will show, this is not trivial since inclusion of higher order terms generates an intractable optimization problem. We propose a novel approach that addresses this issue and leads to a computationally efficient technique. A second contribution of the paper is to apply the optimization method proposed in [14, 15] for the first time to SWI. Inclusion of the higher order terms substantially improves the results, as observed visually and measured quantitatively by the signal to noise ratio (SNR).

This research is supported in part by Grant No. 504310 from the Natural Science and Engineering Research Conference (NSERC), Canada.

2. ESTIMATION OF TISSUE DISPLACEMENT FIELD

Assume $I_1(i,j)$ and $I_2(i,j)$ are two successive ultrasound frames prior to and after undergoing deformation. Symbol I denotes the intensity of the discretized sample (referred to as a pixel) of the image with $i = 1, \cdots, m$ and $j = 1, \cdots, n$ representing the axial and lateral locations of the pixel. The goal of the tracking method is to find two matrices A and L such that their $(i,j)^{\text{th}}$ elements, i.e., $a(i,j) \in A$ and $l(i,j) \in L$ provide estimates of the axial and lateral displacement for pixel (i,j). In Subsection 2.1, we review related work in dynamic programming (DP) [15], which calculates integer displacements for all samples given $I_1(i,j)$ and $I_2(i,j)$. DP is an efficient method for global optimization [16] and has been used extensively in computer vision including solving for optimal deformable models. In Subsection 2.2, we introduce analytic minimization (AM) [14], which takes the integer output values of the DP stage and estimates the displacements at a subpixel level in both axial and lateral directions using a hierarchical search approach. Subsection 2.3 introduces our proposed method based on a refinement of the AM approach that computes the displacement estimates more accurately.

2.1. Dynamic Programming

In order to present the general DP formulation [17], we consider a single column j (an RF-line) of the image $I_1(i,j)$ prior to deformation. Let a_i and l_i denote the axial and lateral displacement of the i^{th} sample of the RF-line in column j. In the DP elastography, a regularized cost function is generated by adding the prior of displacement continuity (the regularization term) to an amplitude similarity term. For column j, the displacement continuity term is given by

$$R(a_i, l_i, a_{i-1}, l_{i-1}) = \alpha_a (a_i - a_{i-1})^2 + \alpha_l (l_i - l_{i-1})^2, \quad (2)$$

which restricts the displacement of the sample i (i.e. a_i and l_i) to be similar to the displacement of the previous sample $i-1$ (i.e., a_{i-1} and l_{i-1}). Symbols α_a and α_l are axial and lateral regularization weights, respectively, while $R(a_i, l_i, a_{i-1}, l_{i-1})$ indicates the dependency of a_i and l_j on j. The regularized cost function as formulated in [15] for column j is then generated as

$$C_j^{(p)}(a_i, l_i, i) = \big[I_1(i,j) - I_2(i + a_i, j + l_i)\big]^2 + \min_{d_a, d_l} \Big(\frac{C_j^{(p)}(d_a, d_l, i\text{–}1) + C_{j-1}^{(p)}(d_a, d_l, i)}{2} + R(a_i, l_i, a_{i-1}, l_{i-1}) \Big) \quad (3)$$

where d_a and d_l are displacement variables in the axial and lateral directions, and the superscript p refers to the pixel displacement estimation (as opposed to subpixel). Set $\{d_a, d_l\}$ are the optimization parameters used to minimize the term within the bracket. After calculating $C_j^{(p)}$, for $i = 2, \cdots, m$, it is minimized at $i = m$ with respect to a_m and l_m. The a_i and l_i values that have minimized the cost function at $i = m$ are then traced back to $i = 1$ resulting in integer values of a_i and l_i for all samples of j^{th} line. The process is continued for the next line $(j+1)^{\text{th}}$ line until the integer valued displacements for the entire image are calculated.

2.2. Analytic Minimization (AM)

In the previous work [14], integer displacement estimates in the axial direction a_i and in the lateral direction l_i for $i = 1 \cdots m$ samples of an RF-line are calculated. The process starts with a line in the middle of the image, referred to as the seed line, and repeated to the neighbouring lines until the entire image is covered. To estimate the subsample displacements, the new cost function is introduced

$$C_j^{(s)}(\Delta a_1, \cdots, \Delta a_m, \Delta l_1, \cdots, \Delta l_m) = \sum_{i=1}^{m} \Big\{ \big[I_1(i,j) - I_2(i + a_i + \Delta a_i, j + l_i + \Delta l_i)\big]^2 + \alpha (a_i + \Delta a_i - a_{i-1} - \Delta a_{i-1})^2 + \beta_a (l_i + \Delta l_i - l_{i-1} - \Delta l_{i-1})^2 + \beta_l (l_i + \Delta l_i - l_{i,j-1})^2 \Big\}, \quad (4)$$

where $I(i,j)$ is the i^{th} sample on the j^{th} RF-line, α, β_a and β_l are regularization weights, and superscript s refers to subpixel displacement estimation. To simplify the notation, we have dropped the index j in terms a_i and l_i in Eq. (4). Therefore, terms a_i, l_i, Δa_i and Δl_i stand for $a_{i,j}$, $l_{i,j}$, $\Delta a_{i,j}$ and $\Delta l_{i,j}$. Symbol $l_{i,j-1}$ is the lateral displacement of the previous RF-line. Note that $l_{i,j-1}$ denotes the total lateral displacement of the previous line, i.e., when the displacement of the $(j-1)^{\text{th}}$ line was being calculated and $l_{i,j-1}$ was updated with $l_{i,j-1} + \Delta l_{i,j-1}$.

Eq.(4) is nonlinear because the variables Δa and Δl appear inside the function I_2. A typical RF dataset involves around $m = 2000$ samples per line leading to 4000 unknowns in Eq.(4). Consequently, optimizing the cost function in Eq. (4) is computationally intensive and cannot be performed in real-time. Previously in [18], we have proposed to approximate the summation term in Eq.(4) involving I_2 with the following first order Taylor series expansion

$$I_2(i + a_i + \Delta a_i, j + l_i + \Delta l_i) \approx I_2(i + a_i, j + l_i) + \Delta a_i I'_{2,a} + \Delta l_i I'_{2,l}, \quad (5)$$

where $I'_{2,a}$ and $I'_{2,l}$ are, respectively, the axial and lateral derivatives of I_2. Substituting the above expression in Eq. (4) results in a quadratic equation. In the matrix-vector format, the coefficient matrix is sparse. Eq (4) can be optimized in about a millisecond on a typical desktop computer.

2.3. Proposed Approach: Higer-order Analytic Minimization

In the proposed higher-order analytic minimization (HAM) approach, we modify the AM method to calculate subsample axial and lateral displacement fields with higher accuracy. In order to achieve this, the cost function in Eq. (4) is optimized using second order Taylor expansion of $I_2(i + a_i + \Delta a_i, j + l_i + \Delta l_i)$ instead of first order approximation performed in previous work (AM). The outline of our algorithm is provided below.

1. Perform DP (Eq. (3)) to calculate the integer values of the displacements for the one seed RF-line. Then calculate linear interpolation of the integer valued displacements to find better initial subsample displacement for the seed RF-line.
2. For the seed RF-line, minimize the regularized cost function HAM as elaborated in Section 2.3 to obtain the subpixel displacement of the seed line.
3. Repeat the previous step for RF lines to the right and left of the seed RF-line using the HAM method considering the displacement of the previous line as the initial displacement estimate for the current line.

Assume that a_i and l_i are the initial displacement estimates in the axial and lateral directions for $i = 1 \cdots m$ samples of an RF-line. For the seed-line, a_i and l_i are the linear interpolation of the integer DP displacements. For the rest of the lines, a_i and l_i are the displacements of the previous line. The purpose of the HAM, similar to AM,

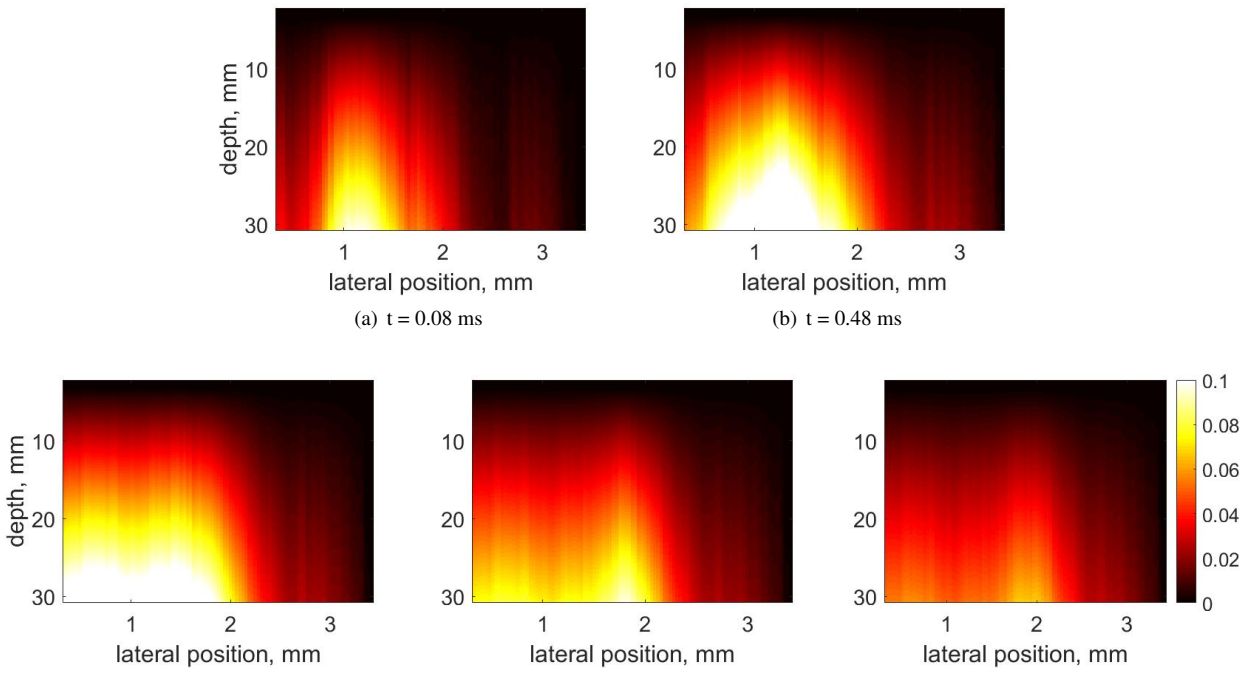

(a) t = 0.08 ms (b) t = 0.48 ms

(c) t = 0.8 ms (d) t = 1.12 ms (e) t = 1.44 ms

Fig. 1. Axial displacement fields of CIRS phantom experiment using the HAM method for five frames after an excitation. Axes are in mm.

is to find Δa_i and Δl_i values such that (a_i + Δa_i, l_i + Δl_i) gives the axial and lateral displacements at the sample i. The second order Taylor expansion contains Δa_i^2 and Δl_i^2. Therefore, on one hand, substituting these terms into into Eq. (4) results in a polynomial cost function of order 4. On the other hand, for an RF data of length 2000, Eq. (4) has 4000 variables. Optimization of such a high dimensional nonlinear cost function is computationally expensive. For a practically feasible implementation, we adopt the following approach

$$\begin{aligned} &C_j(\Delta a_1, \cdots, \Delta a_m, \Delta l_1, \cdots, \Delta l_m) = \\ &\sum_{i=1}^{m} \Big\{ w_{i,j}[I_1(i,j) - I_2(i + a_i + \Delta a_i, j + l_i + \Delta l_i)]^2 \\ &+ \alpha(a_i + \Delta a_i - a_{i-1} - \Delta a_{i-1})^2 + \beta_a(l_i + \Delta l_i - l_{i-1} - \Delta l_{i-1})^2 \\ &+ \beta_l(l_i + \Delta l_i - l_{i,j-1})^2 \Big\}, \end{aligned} \tag{6}$$

$$\text{where} \quad w_{i,j} = \frac{1}{\epsilon + |I''_{2,a}(i,j)| + |I''_{2,l}(i,j)|} \tag{7}$$

where ϵ a small positive constant to prevent the denominator from becoming zero. Symbols $|I''_{2,a}(i,j)|$ and $|I''_{2,l}(i,j)|$ denote the absolute values of second-order derivatives in the axial and lateral directions respectively. Intuitively, incorporating $w_{i,j}$ in the principal cost function Eq. (6) penalizes samples that have a high second-order derivative. This is because we only use first order Taylor expansion to simplify the nonlinear cost function, and this approximation is only good when the second-order derivative is small.

If the displacement estimate of the previous line is not accurate, it will affect the displacement of the next line through the last term in the right hand side of Eq. (6). We avoid propagating this error to the neighbouring RF lines by setting β_l as follows

$$\beta_l = \frac{\beta_l}{1 + |r_{i,j-1}|} \tag{8}$$

where $r_{i,j-1}$ is the residual associated with the displacement of the i^{th} sample of the previous line. Note β_l will be small when there is a large residual and its influence on the next line will be small.

The optimal (Δa_i,Δl_i) values will make the partial derivatives of C_j with respect to Δa_i and Δl_i equal to zero. Setting $\partial C_j/\partial \Delta a_i = 0$ and $\partial C_j/\partial \Delta l_i = 0$, for $i = 1 \cdots m$, and stacking the $2m$ unknowns in $\Delta d = [\Delta a_1, \Delta l_1, \Delta a_2, \Delta l_2, \cdots, \Delta a_m, \Delta l_m]^T$ and $2m$ initial estimates in $d = [a_1, l_1, a_2, l_2, \cdots, a_m, l_m]^T$ gives

$$(I'^2_2 + D_1 + D_2)\Delta d = I'_2 e - D_1 d \tag{9}$$

where $I'^2_2 = \text{diag}(J'^2(1) \cdots J'^2(m))$ is a symmetric tridiagonal matrix of size $2m \times 2m$ with

$$J'^2(i) = \begin{bmatrix} I'^2_{2,a} & I'_{2,a} I'_{2,l} \\ I'_{2,a} I'_{2,l} & I'^2_{2,l} \end{bmatrix} \tag{10}$$

blocks on its diagonal entries where $I'_{2,a}$ and $I'_{2,l}$ are the derivatives of I_2 at point $(i + a_i, j + l_i)$ in the axial and lateral directions and

$$D_1 = \begin{bmatrix} \alpha & 0 & -\alpha & 0 & 0 & 0 & \cdots & 0 \\ 0 & \beta_\alpha & 0 & -\beta_\alpha & 0 & 0 & \cdots & 0 \\ -\alpha & 0 & 2\alpha & 0 & -\alpha & 0 & \cdots & 0 \\ 0 & -\beta_\alpha & 0 & 2\beta_\alpha & 0 & -\beta_\alpha & \cdots & 0 \\ 0 & 0 & -\alpha & 0 & 2\alpha & 0 & \cdots & 0 \\ \vdots & & & & & & \ddots & \\ 0 & 0 & 0 & \cdots & -\alpha & 0 & \alpha & 0 \\ 0 & 0 & 0 & \cdots & 0 & -\beta_\alpha & 0 & \beta_\alpha \end{bmatrix} \tag{11}$$

and $D_2 = \text{diag}(0, \beta'_l, 0, \beta'_l, \cdots, 0, \beta'_l)$ is a diagonal matrix with dimensions $2m \times 2m$.

$$\begin{aligned} &I'_2 = w_{i,j} \times \\ &\text{diag}(I'_{2,a}(1), I'_{2,l}(1), I'_{2,a}(2), I'_{2,l}(2), \cdots I'_{2,a}(m), I'_{2,l}(m)) \end{aligned} \tag{12}$$

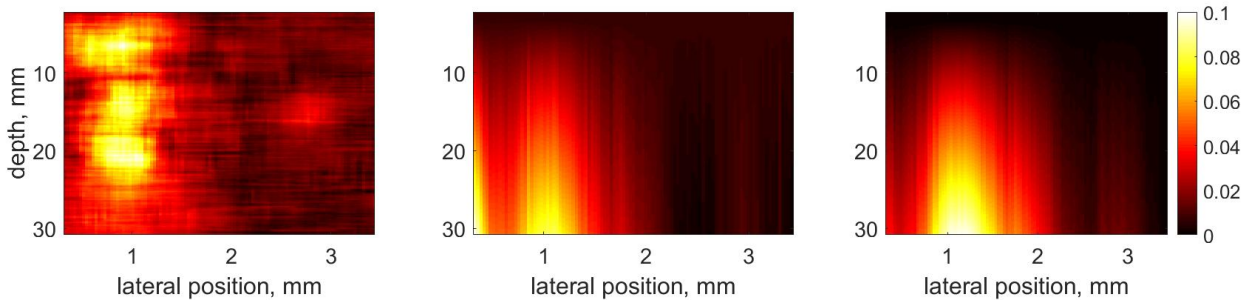

(a) NCC (b) AM (c) HAM

Fig. 2. Axial Displacement fields of CIRS Phantom experiment using the HAM, AM and NCC methods. The frames are estimated for t = 0.08 ms after the excitation occurs. Axes are in mm.

Table 1. SNR values for the shear-wave velocity across the phantom using three HAM, AM and NCC methods. The SNR improvement in in comparison with the NCC method is provided.

	NCC	AM	HAM
SNR	3.08	3.37	3.74
%age of SNR improvement	-	9	21

where $I'_{2,a}(i)$ and $I'_{2,l}(i)$ are calculated at point $(i+a_i, j+l_i)$, and $e = [e_1 e_1 e_2 e_2 \cdots e_m]^T, e_i = w_{i,j}(I_1(i,j) - I_2(i+a_i, j+l_i))$. Having $\Delta d = [\Delta a_1, \Delta l_1, \Delta a_2, \Delta l_2, \cdots, \Delta a_m, \Delta l_m]^T$ and $2m$ initial estimates in $d = [a_1, l_1, a_2, l_2, \cdots, a_m, l_m]$, we will find $2m$ axial and lateral displacements for $i = 1 \cdots m$ for j^{th} line. Afterward, we follow the same procedure for the neighbouring line and consider the calculated displacement on j^{th} line as initial value. Repeating this algorithm gives us both axial and lateral displacement values for the entire image.

3. EXPERIMENTAL RESULTS

Real experimental phantom data was used to assess the precision and accuracy of the proposed HAM method. The results were compared with the AM and normalized cross correlation (NCC) based approaches. The RF data is acquired from an CIRS 049A experimental phantom using a transducer of type L3-8 operating at the central frequency of 5.3 MHz, comprising of 128 elements, and with a pitch of 0.03 mm. The Central element of the push beam aperture is 31^{th} element out of 64 active elements at a focal depth of 20 mm. For data acquisition, the spatial resolution in the lateral and axial directions are 0.03 and 0.077 mm, respectively.

Since the wave inside the tissue is of transversal nature that propagates perpendicular to the displacement [19], only axial displacement fields are assessed in this section. Figure 1 shows five axial displacement frames of the same tissue but at different times of propagation. As show in the figure, the wave starts propagating from the ROE to all sides. The axial displacement fields computed using HAM, AM and NCC methods for the experimental phantom data are shown in Figure 2. Since the HAM method incorporated more information as compared to AM, a better performance is observed. Both methods are fast enough and suitable for real-time implementation and have approximately the same computational complexity. To find displacement field for an image of size 455×128 using HAM and AM, arround one second is required; whereas, that is around 30 s by applying 90 % overlapping using NCC. The tuneable parameters of the HAM method are set to $\alpha = 800$, $\beta_a = 1$ and $\beta_l = 1$ to achieve the best results while the same parameters are set to 20, 1 and 1, respectively, in AM.

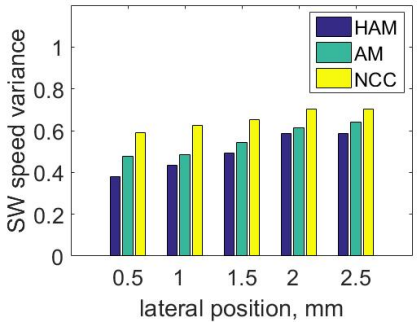

Fig. 3. SW (Shear wave) speed variance in the tissue-mimicking phantom calculated using 20 consecutive displacement frames.

Phantom Young's moduli (7 KPa) is used to estimate the shear wave speed as the ground truth. The experimental phantom is homogeneous, and as such, it has a uniform shear-wave speed. Therefore, in order to validate the results, we calculate shear-wave velocity to compare NCC, AM and HAM. As expected, the shear-wave propagates inside a uniform tissue with a constant speed [20]. Figure 3 shows the standard deviation calculated for speed of shear-wave using the time-to-peak (TOF) algorithm [21] across the lateral position. The HAM method yields a substantially smaller variance in the shear wave-speed as compared to NCC and AM, illustrating superior performance. Similar results were observed for a variety of different setups.

4. CONCLUSION

The paper proposes a regularized cost function to track small displacements in shear-wave elastography. We show that direct incorporation of the second-order derivatives into the cost function makes the optimization computationally intractable. To address this issue, we developed an approach based on higher-order analytical minimization that improves the accuracy of the estimate for tissue displacement fields as verified in real-time experiments based on tissue-mimicking phantom. The proposed method is computationally efficient and is suitable for real-time implementation on commercial ultrasound machines.

5. REFERENCES

[1] S. Catheline, F. Wu, and M. Fink, "A solution to diffraction biases in sonoelasticity: the acoustic impulse technique," *The Journal of the Acoustical Society of America*, vol. 105, no. 5, pp. 2941–2950, 1999.

[2] J. Ophir, B. Garra, F. Kallel, E. Konofagou, T. Krouskop, R. Righetti, and T. Varghese, "Elastographic imaging," *Ultrasound in medicine & biology*, vol. 26, pp. S23–S29, 2000.

[3] L. Sandrin, M. Tanter, J.-L. Gennisson, S. Catheline, and M. Fink, "Shear elasticity probe for soft tissues with 1-d transient elastography," *IEEE transactions on ultrasonics, ferroelectrics, and frequency control*, vol. 49, no. 4, pp. 436–446, 2002.

[4] D. B. Plewes, J. Bishop, A. Samani, and J. Sciarretta, "Visualization and quantification of breast cancer biomechanical properties with magnetic resonance elastography," *Physics in medicine and biology*, vol. 45, no. 6, p. 1591, 2000.

[5] D. D. Steele, T. L. Chenevert, A. R. Skovoroda, and S. Y. Emelianov, "Three-dimensional static displacement, stimulated echo nmr elasticity imaging," *Physics in Medicine and Biology*, vol. 45, no. 6, p. 1633, 2000.

[6] A. P. Sarvazyan, O. V. Rudenko, S. D. Swanson, J. B. Fowlkes, and S. Y. Emelianov, "Shear wave elasticity imaging: a new ultrasonic technology of medical diagnostics," *Ultrasound in medicine & biology*, vol. 24, no. 9, pp. 1419–1435, 1998.

[7] W. F. Walker, F. J. Fernandez, and L. A. Negron, "A method of imaging viscoelastic parameters with acoustic radiation force," *Physics in medicine and biology*, vol. 45, no. 6, p. 1437, 2000.

[8] J. Bercoff, M. Tanter, S. Chaffai, and M. Fink, "Ultrafast imaging of beamformed shear waves induced by the acoustic radiation force. application to transient elastography," in *Proceedings of the 2002 IEEE Ultrasonics Symposium*, vol. 2, 2002, pp. 1899–1902.

[9] K. Nightingale, S. McAleavey, and G. Trahey, "Shear-wave generation using acoustic radiation force: in vivo and ex vivo results," *Ultrasound in medicine & biology*, vol. 29, no. 12, pp. 1715–1723, 2003.

[10] K. Nightingale, M. S. Soo, R. Nightingale, and G. Trahey, "Acoustic radiation force impulse imaging: in vivo demonstration of clinical feasibility," *Ultrasound in medicine & biology*, vol. 28, no. 2, pp. 227–235, 2002.

[11] C. Sumi, "Usefulness of ultrasonic strain measurement- based shear modulus reconstruction for diagnosis and thermal treatment," *IEEE Trans. Ultrason. Ferroelectr. Freq. Control*, vol. 52, no. 10, pp. 1670 – 1689, Oct. 2005.

[12] M. Friedrich-Rust, K. Wunder, S. Kriener, F. Sotoudeh, S. Richter, J. Bojunga, E. Herrmann, T. Poynard, C. F. Dietrich, J. Vermehren *et al.*, "Liver fibrosis in viral hepatitis: noninvasive assessment with acoustic radiation force impulse imaging versus transient elastography 1," *Radiology*, vol. 252, no. 2, pp. 595–604, 2009.

[13] M. L. Palmeri, S. A. McAleavey, G. E. Trahey, and K. R. Nightingale, "Ultrasonic tracking of acoustic radiation force-induced displacements in homogeneous media," *IEEE transactions on ultrasonics, ferroelectrics, and frequency control*, vol. 53, no. 7, pp. 1300–1313, 2006.

[14] H. Rivaz, E. M. Boctor, M. A. Choti, and G. D. Hager, "Real-time regularized ultrasound elastography," *IEEE transactions on medical imaging*, vol. 30, no. 4, pp. 928–945, 2011.

[15] H. Rivaz, E. Boctor, P. Foroughi, R. Zellars, G. Fichtinger, and G. Hager, "Ultrasound elastography: a dynamic programming approach," *Medical Imaging, IEEE Transactions on*, vol. 27, no. 10, pp. 1373–1377, 2008.

[16] A. A. Amini, T. E. Weymouth, and R. C. Jain, "Using dynamic programming for solving variational problems in vision," *IEEE Transactions on pattern analysis and machine intelligence*, vol. 12, no. 9, pp. 855–867, 1990.

[17] R. E. Bellman and S. E. Dreyfus, *Applied dynamic programming*. Princeton university press, 2015.

[18] H. Rivaz, E. M. Boctor, M. A. Choti, and G. D. Hager, "Ultrasound elastography using multiple images," *Medical image analysis*, vol. 18, no. 2, pp. 314–329, 2014.

[19] J.-L. Gennisson, T. Deffieux, E. Macé, G. Montaldo, M. Fink, and M. Tanter, "Viscoelastic and anisotropic mechanical properties of in vivo muscle tissue assessed by supersonic shear imaging," *Ultrasound in medicine & biology*, vol. 36, no. 5, pp. 789–801, 2010.

[20] M. L. Palmeri, M. H. Wang, J. J. Dahl, K. D. Frinkley, and K. R. Nightingale, "Quantifying hepatic shear modulus in vivo using acoustic radiation force," *Ultrasound in medicine & biology*, vol. 34, no. 4, pp. 546–558, 2008.

[21] N. C. Rouze, M. H. Wang, M. L. Palmeri, and K. R. Nightingale, "Robust estimation of time-of-flight shear wave speed using a radon sum transformation," *IEEE transactions on ultrasonics, ferroelectrics, and frequency control*, vol. 57, no. 12, pp. 2662–2670, 2010.